Mendeleev Commun., 2027, **37**, JUST ACCEPTED

Received 03.09.26
Revised 12.10.26

26/8190

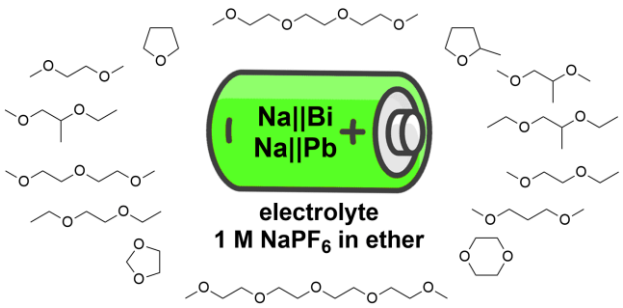
Systematic physicochemical profiling of ether-based electrolytes for sodium-ion batteries

Irina V. Kutovaya,[a] Alena I. Komayko,[a] Mikhail D. Agapkin,[a] Arina A. Elagina,[a] Rustem R. Gamirov,[b] Stanislav S. Fedotov[a] and Olga I. Shmatova *[a]

[a] *Center for Energy Science and Technology, Skolkovo Institute of Science and Technology, 121205 Moscow, Russian Federation. E-mail: o.shmatova@skoltech.ru*
[b] *Alexander Butlerov Institute of Chemistry, Kazan Federal University, 420008 Kazan, Russian Federation*

DOI: 10.71267/mencom.8190

Ten ether-based $NaPF_6$ electrolytes were systematically characterized, analyzing solvation, ionic conductivity, electrochemical stability, and interfacial kinetics. Tests in Na||Bi and Na||Pb cells revealed diglyme, 1,2-dimethoxyethane, and 1,2-dimethoxypropane as superior solvents.



Keywords: sodium-ion batteries, electrolytes, ethers, ionic conductivity, low-temperature, metal anodes.

The global energy transition demands a new generation of energy storage technologies that are not only sustainable and scalable but also chemically diverse, economically resilient, and fundamentally adaptable to evolving grid and mobility needs.[1-4] Sodium-ion batteries (SIBs) have emerged as a strategically vital complementary technology to lithium-ion batteries (LIBs), offering a compelling combination of abundant raw materials, reduced geopolitical risk, and lower manufacturing costs[5] with sodium being significantly more plentiful and geographically distributed than lithium, enabling potential reductions in raw material expenses by 30–40%.[6,7] While LIBs continue to dominate high-energy-density applications, their reliance on graphite anodes and carbonate-based electrolytes imposes intrinsic limitations in terms of anode kinetics, interfacial stability, and material compatibility with high-capacity alloying anodes.[8,9] In contrast, SIBs provide a uniquely flexible platform for exploring novel anode chemistries beyond intercalation hosts.[10-12]. Metals such as bismuth and lead have garnered attention due to their high theoretical capacities (~385 (Bi) and ~485 (Pb) $mAh \cdot g^{-1}$) and favorable sodium storage mechanisms via reversible alloying/dealloying.[13,14] These metals enable high areal capacities and operate via distinct charge storage pathways, offering the potential for both higher energy density and improved rate capability.[15-17]

A critical enabler of these advanced anode systems is the electrolyte.[18-20] Conventional carbonate-based electrolytes, that were optimized for lithium intercalation, often promote the formation of fragile solid-electrolyte interphases (SEI),[21] and possess limited compatibility with alloying anodes that undergo large volume changes during cycling.[22,23] Ether-based solvents present a fundamentally different solvation landscape: their weakly coordinating nature enhances Na^+ mobility and reduces desolvation energy.[24-26] These properties are especially advantageous when paired with high-capacity metal anodes, where stable interfacial kinetics are paramount to suppressing dendrite formation, minimizing side reactions, and sustaining long-term cyclability.[27] Despite these advantages, the physico-chemical behavior of ether electrolytes in conjunction with bismuth and lead anodes remains incompletely characterized.[28-30] Key parameters including ion-pairing, viscosity-conductivity trade-offs, and low-temperature properties require systematic investigation to enable rational electrolyte design for practical use.

This work presents a detailed physico-chemical evaluation of different ether-based electrolytes for high-capacity bismuth and lead anodes in SIBs. By integrating spectroscopic and electrochemical characterization techniques, we examined a series of ten electrolytes in order to elucidate the optimal solvents for efficient ion transport and anode–electrolyte compatibility. The electrolytes 1M $NaPF_6$ in 1,2-dimethoxyethane and diglyme were found to possess the most balanced physico-chemical properties at room temperature, while 1,2-dimethoxypropane-based was found to be superior at sub-zero temperatures, which allows to consider it as a prospective candidate for all-climate SIBs.

For this study, we selected the readily available $NaPF_6$ as the sodium salt and evaluated a library of 14 ethereal solvents bearing optimal physical properties (Table S1), including glymes (1,2-dimethoxyethane DME, diglyme DiG, triglyme TriG, tetraglyme TeG), structural DME homologs (1-ethoxy-2-methoxyethane EME, 1,2-dimethoxypropane 1,2-DMP, 1,3-dimethoxypropane 1,3-DMP, 1-ethoxy-2-methoxypropane EMP, 1,2-diethoxyethane DEE, 1,2-diethoxypropane DEP) and cyclic ethers (tetrahydrofuran THF, 2-methyltetrahydrofuran MeTHF, 1,3-dioxolane DOL, 1,4-dioxane DON). Of these, DOL, DON, and TriG failed to dissolve $NaPF_6$, while MeTHF exhibited chemical instability upon prolonged contact with the salt. The remaining ten solvents were used to formulate 1M

© Mendeleev Communications.

$NaPF_6$ electrolytes (Fig. 1a). We assessed their suitability for practical applications by measuring viscosity and ionic conductivity (Fig. 1b): while all formulations exhibited sufficient ionic conductivity over 1MS/cm, electrolytes based on DEP (10.99 cP) and TeG (13.03 cP) displayed prohibitively high viscosities, which may impede ion mobility and limit rate performance of SIBs.

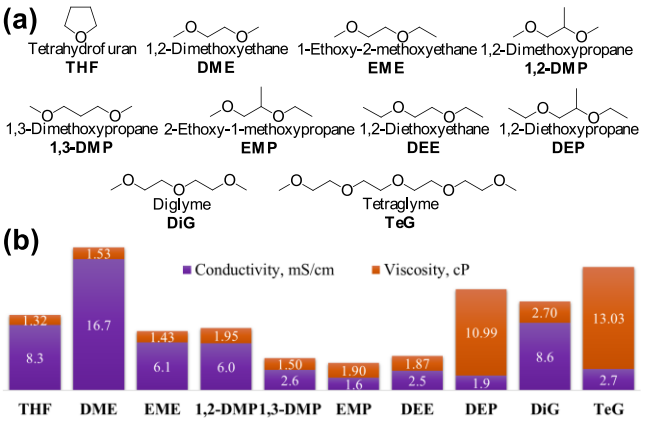


Figure 1 *(a)* Chemical structures of used ether solvents; *(b)* viscosity and ionic conductivity of electrolytes consisting of 1M $NaPF_6$ in ether.

Analysis of diffusion coefficients via DOSY NMR (Fig. 2a, Table S2, Fig. S7-S30) revealed distinct solvation structures: Na^+ coordination numbers averaged 2.39 for DME, 2.29 for EMP, 2.23 for EME, 1.90 for DiG, 1.88 for 1,2-DMP, and 1.65 – 1.64 for 1,3-DMP and DEE (Fig 2a). Due to differences in the oxygen donor atom count, which is critical for direct comparison, THF (1O) and DiG (3O) were excluded from the solvation strength ranking, which instead prioritized ethers with two oxygen atoms: DME > EMP > EME > 1,2-DMP > 1,3-DMP ≈ DEE. Notably, EMP exhibited unexpectedly low ionic conductivity despite its high coordination number. This suggests that steric constraints from its branched alkyl groups limit bidentate coordination, resulting in a more voluminous and less mobile solvation shell.

Ionic conductivity measurements (Fig. 2b) of the chosen eight ether-based electrolytes show that, at 25 °C, DME exhibits the highest conductivity (~16.7 mS/cm), nearly twice that of the second-best solvent, DiG (8.6 mS/cm). However, upon cooling below 0°C, DME's performance deteriorated sharply due to $NaPF_6$ precipitation, reducing effective concentration (Fig. 2b, Table S3). In contrast, 1,2-DMP maintained >2 mS/cm even at -40°C, demonstrating superior low-temperature resilience. DiG, EME, and THF exhibited salt precipitation below -10°C, -20°C, and -30°C, respectively. The 1,3-DMP-, DEE-, and EMP-based electrolytes demonstrated poor ionic conductivity (<3 mS/cm) even at 25 °C. To probe the role of anion in ion transport, we compared DiG-based electrolytes with $NaPF_6$ and $NaBF_4$. $NaPF_6$ delivered fivefold higher ionic conductivity than $NaBF_4$ at 25°C, which aligns with prior studies and is attributed to PF_6^- 's weaker ion pairing and enhanced dissociation (Fig. S31).[31] To identify the optimal salt concentration, we evaluated five ether solvents across 0.5 – 2.0 M $NaPF_6$ (Fig. S32, Table S4). Ionic conductivity and viscosity both increased nonlinearly with concentration, with DME and DiG reaching >80% of their maximum conductivity at 1M (Table S4). Balancing performance, stability, and practicality, 1M $NaPF_6$ was selected as the standard concentration for all subsequent electrochemical evaluations.

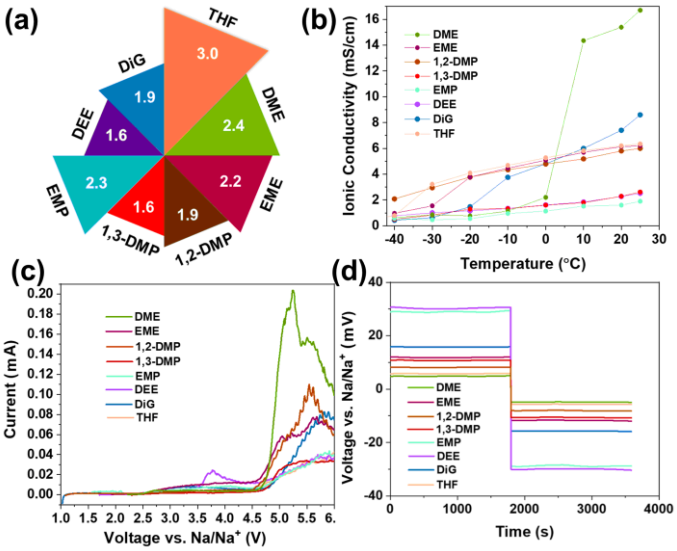


Figure 2 Properties of 1M $NaPF_6$/ ether electrolytes: (*a*) Na^+ coordination number calculated via DOSY NMR. (*b*) Ionic conductivities at temperatures -40 - 25°C. (*c*) Linear-sweep voltammetry in Na||stainless steel cells. *(d)* Overpotential in Na||Na cells with current density 2 mA/cm^2.

Electrochemical stability was examined via linear sweep voltammetry (0.1MV/s, vs. Na^+/Na, Fig. 2c). Oxidative decomposition began at 4.6 – 4.7 V for most solvents, with EMP and 1,3-DMP showing the highest stability (>4.7 V), while THF and DiG degraded earlier (~4.6 V). DEE displayed a premature oxidation onset at ~3.5 V, likely due to its longer alkyl chain enhancing electron density at ether oxygens. Galvanostatic tests for symmetric Na||Na cells revealed strong correlations between solvation structure and interfacial kinetics (Fig. 2d). DME and THF exhibited the lowest overpotentials (2.0 – 5.7 mV from 0.5 to 2 mA/cm^2), consistent with their compact solvation shells and high mobility (Table S5). In contrast, DEE and EMP showed the highest polarization (~13 – 30 mV), aligning with their lower conductivity and hindered ion transport.

Galvanostatic cycling in Na||Bi and Na||Pb half-cells revealed stark differences across electrolytes. Electrolytes based on DME, DiG, and 1,2-DMP delivered superior performance in both capacity retention and Coulombic efficiency (CE) (Fig. 3, Table S6). In Na||Bi cells, these three electrolytes retained 94.9%, 99.4%, and 97.1% of initial capacity, respectively after 500 cycles, with average CEs of 99.96% (DME), 99.95% (DiG), and 99.94% (1,2-DMP), approaching ideal reversibility. In contrast, EME-, DEE-, and 1,3-DMP-based electrolytes showed moderate performance: capacity retention of 94 – 95% after 500 cycles, with CEs of 99.86%, 99.92%, and 99.91%, respectively. EMP underperformed dramatically, retaining only ~80% capacity, while THF exhibited poor CE (99.81%). Representative charge/discharge curves at cycles 1, 25, and 500 are shown in Figure S33. The anodes were all-metal Bi and Pb layers. Their preparation and morphology before cycling and after 10 cycles in a diglyme-based electrolyte were described previously.[32]

© Mendeleev Communications.

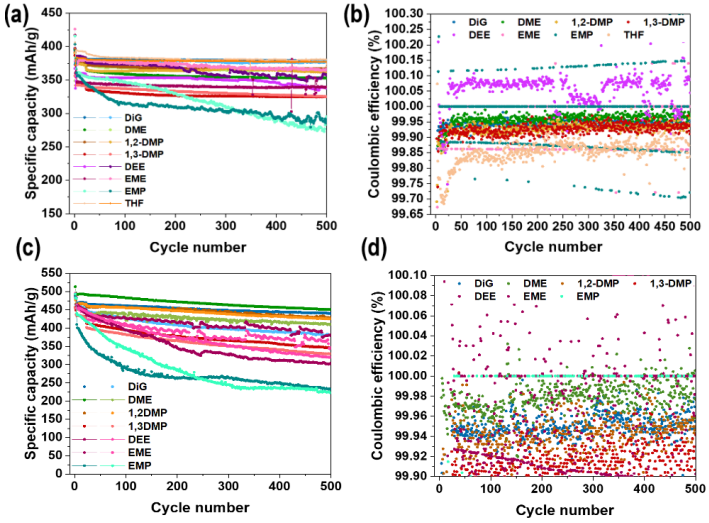


Figure 3 Capacity retention *(a, c)* and Coulombic efficiency *(b, d)* of Na||Bi and Na||Pb half-cells. First three cycles charge/discharge rate 0.1C, next 20 cycles – 0.5C, remaining cycles – 1C (385 and 485 mA g^{-1} for Bi and Pb, respectively).

Similar trends were observed in Na||Pb cells (Fig. 3c, d): DME, DiG, and 1,2-DMP maintained >88% capacity retention after 500 cycles with CEs of 99.97%, 99.95%, and 99.93%. EME, DEE, and 1,3-DMP showed reduced reproducibility and lower average capacity retention (68–78%) with efficiencies near ~99.90%. EMP again lagged behind, delivering just 53.7% capacity retention. These performance disparities were directly correlated with overpotential in symmetric Na||Na cells, where DEE and EMP exhibited the highest polarization confirming their kinetically hindered sodium plating/stripping behaviour.

In summary, a comprehensive physicochemical characterization of SIB electrolytes based on $NaPF_6$ and ten different ether solvents was performed. The solvation shell structures were elucidated, and the temperature-dependent ionic conductivity and concentration-dependent viscosity and ionic conductivity were determined. Furthermore, the redox stability and overpotentials were investigated. The electrolytes were galvanostatically tested in Na||Bi and Na||Pb using all-metal anodes. The best capacity retention and average CE were achieved with DiG-, DME-, and 1,2-DMP-based electrolytes, with the performance discrepancy being particularly pronounced in the case of the lead anode.

The research was supported by an R&D contract with Metalion JSC.

Online Supplementary Materials

Supplementary data associated with this article can be found in the online version at doi: 10.71267/mencom.8190.

References

1 A. Ibn Amzad Anil, M. R. Al Muttaki, S. Afrin and S. Hasan, *Energy Convers. Manage.:X*, 2026, **30**, 101771; https://doi.org/10.1016/j.ecmx.2026.101771.

2 X. Liu, W. Li, X. Guo, B. Su, S. Guo, Y. Jing and X. Zhang, *Sustainability*, 2025, **17**, 8316; https://doi.org/10.3390/su17188316.

3 F. H. Malik, G.A. Hussain, Y. M. S. Alsmadi, Z. M. Haider, W. Mansoor and M. Lehtonen, *Sustainability*, 2025, **17, 4097;** https://doi.org/10.3390/su17094097.

4 G. Özsin, *Turk. J. Chem., 2025, 49, 1-28*; https://doi.org/10.55730/1300-0527.3707.

5 M. M. Mashfy, T. A. Alvy, N. Hossain, M. A. Haque, F. T. Mohsin, T. Sharmin and M. Nasim, *Next Energy*, 2026, **10**, 100478; https://doi.org/10.1016/j.nxener.2025.100478.

6 R. Shahazi, M. Akther, J. Malo, M. Dayna, J. Paul, M. R. Uddin and M. M. Alam, *Mater. Technol. Rep.*, 2025, **3(1)**, 2951; https://doi.org/10.59400/mtr2951.

7 J. Wang, Y. Wang, D.-H. Seo, T. Shi, S. Chen, Y. Tian, H. Kim and G. Ceder, *Adv. Energy Mater.*, 2020, **10(10)**; https://doi.org/10.1002/aenm.201903968.

8 I. T. Adebanjo, J. Eko, A. G. Agbeyegbe, S. F. Yuk, S. V. Cowart, E. A. Nagelli, F. J. Burpo, J. L. Allen, D. T. Tran, N. Bhattarai, K. Shah, J.-Y. Hwang and H. Hohyun Sun, *Energy Adv.*, 2025, **4**, 820-877; https://doi.org/10.1039/D5YA00065C.

9 B. Vedhanarayanan, J. Nagaraj, K. Arjunan and K. C. S. Lakshmi, *Nanoenergy Adv.*, 2025, **5**, 13; https://doi.org/10.3390/nanoenergyadv5040013.

10 S. Hong, Y. Deng, S. Wan-Hsuan Lin and L. A. Archer, *ACS Energy Lett.*, 2026, **11(3)**, 2553-2580; https://doi.org/10.1021/acsenergylett.5c03890.

11 B. Song, Y. Cheng, G. Zhao, K. Jia, Q. Shi, X. Li, Z. Wang, Y. Zhou, G. Zou and X. Ji, *Adv. Funct. Mater.*, 2025, **35**, 51:e10872; https://doi.org/10.1002/adfm.202510872.

12 A. M. Skundin, T. L. Kulova, I. M. Gavrilin, D. A. Dronova, B. B. Nomozov, E. V. Kovtushenko and Y. O. Kudryashova, Mendeleev Commun., 2026, 36, 350–352; https://doi.org/10.71267/mencom.7918.

13 Y. Wang, X. Xu, F. Li, S. Ji, J. Zhao, J. Liu and Y. Huo, *Batteries*, 2023, **9**, 440; https://doi.org/10.3390/batteries9090440.

14 X. Wang, X. Zhao and L. Wang, *Batteries Supercaps*, 2025, **8**, e202400551; https://doi.org/10.1002/batt.202400551.

15 S. Mukherjee, S. Bin Mujib, D. Soares and G. Singh, *Materials*, 2019, **12**, 1952; https://doi.org/10.3390/ma12121952.

16 M. S. Iyer, P. Rajkumar, B. Sanghavi, G. Parvathy, K. Aravinth, J. Kim, *J. Power Sources*, 2024, **602,** 234379; https://doi.org/10.1016/j.jpowsour.2024.234379.

17 Y. Zhao, A. Manthiram, *Chem. Mater.*, 2015, **27 (8)**, 3096-3101; https://doi.org/10.1021/acs.chemmater.5b00616.

18 N. Aslfattahi, L. Samylingam, M. S. Kiai, K. Kadirgama, V. Kulish, M. Schmirler and Z. Said, *J. Energy Storage*, 2023, **72 Part E**, 108781; https://doi.org/10.1016/j.est.2023.108781.

19 S. Kainat, J. Anwer, A. Hamid, N. Gull and S. M. Khan, *Mater. Chem. Phys.*, 2024, **313**, 128796; https://doi.org/10.1016/j.matchemphys.2023.128796.

20 S. Awasthi, *J. Energy Storage*, 2024, **100 Part A**, 113439; https://doi.org/10.1016/j.est.2024.113439.

21 Y. Li, Z. Ni, J. Geng, Z. Wang, Y. Li, Y. Zhao, H. Shao, Y. Li, S. Xiong and J. Feng, *Adv. Energy Mater.*, 2025, **15(34)**, 2502284; https://doi.org/10.1002/aenm.202502284.

22 R. Tian, M. Xie, and Z. Shi, *Chem. Eur. J.*, 2026, e03628; https://doi.org/10.1002/chem.202503628.

23 L. Zhou, Z. Cao, W. Wahyudi, J. Zhang, J.-Y. Hwang, Y. Cheng, L. Wang, L. Cavallo, T. Anthopoulos, Y.-K. Sun, H. N. Alshareef and J. Ming, *ACS Energy Lett.*, 2020, **5(3)**, 766-776; https://doi.org/10.1021/acsenergylett.0c00148.

24 M. Li, Z. Liu, Y. Zhao, Z. Chen, Y. Zhang and N. Zhang, *Nat. Commun.*, 2026, **17**, 1478; https://doi.org/10.1038/s41467-026-69237-y.

25 Y. Bai, J. Huang, T. Sun, H. Liu, S. Dou and C. Wu, *Energy Storage Mater.*, 2025, **83**, 104706; https://doi.org/10.1016/j.ensm.2025.104706.

26 X. Li, F. Luo, N. Zhou, H. Adenusi, S. Fang, F. Wu, S. Passerini, *Adv. Energy Mater.*, 2025, **15**, 2501272; https://doi.org/10.1002/aenm.202501272.

27 C. Wang, L. Wang, F. Li, F. Cheng, and J. Chen, *Adv. Mater.*, 2017, **29**, 1702212; https://doi.org/10.1002/adma.201702212.

28 X. Zhou, X. Chen, W. Kuang, X. Zhang, X. Wu, X. Chen, C. Zhang, L. Li and S.-L. Chou, *Chem. Sci.*, 2024, **15**, 12189-12199; https://doi.org/10.1039/D4SC03226H.

29 X. Wu, Z. Li, W. Feng, W. Luo, L. Liao, H. Cai, X. Chen, Z. Deng, J. Wu, B. Xing, J. Ren, Z. Lou and L. Mai, *Energy Storage Mater.*, 2024, **66**, 103219; https://doi.org/10.1016/j.ensm.2024.103219.

30 Y. Tan, F. Mo, and H. Li, *Nano-Micro Lett.*, 2025, **17**, 126; https://doi.org/10.1007/s40820-024-01641-9.

31 H. Peng, H. Liu, C. Li, Y. Li, Q. Chen and T. Li, *Chin. Chem. Lett.*, 2025, **36(1)**, 109556; https://doi.org/10.1016/j.cclet.2024.109556.

32 M. D. Agapkin, N. D. Luchinin, S. N. Marshenya, M. V. Zakharkin, E. V. Antipov and S. S. Fedotov, Dokl. Chem., 2026, 528, 146–157; https://doi.org/10.7868/S3034511126030139.

© Mendeleev Communications.

Received: 3rd September 2026; Com. 26/8190

© Mendeleev Communications.